Available online at www.sciencedirect.com
SCIENCE DIRECT®
Journal of Nuclear Materials 347 (2005) 20–30
journal of nuclear materials
www.elsevier.com/locate/jnucmat

Thermal property characterization of a titanium modified austenitic stainless steel (alloy D9)

Aritra Banerjee [a], S. Raju [a,*], R. Divakar [a], E. Mohandas [a], G. Panneerselvam [b], M.P. Antony [b]

[a] *Physical Metallurgy Section, Materials Characterisation Group, Indira Gandhi Centre for Atomic Research, Kalpakkam 603 102, India*
[b] *Fuel Chemistry Division, Indira Gandhi Centre for Atomic Research, Kalpakkam 603 102, India*

Received 17 November 2004; accepted 13 June 2005

Abstract

The temperature dependence of lattice parameter and enthalpy increment of alloy D9, a titanium modified nuclear grade austenitic stainless steel were studied using high temperature X-ray diffraction and inverse drop calorimetry techniques, respectively. A smooth variation of the lattice parameter of the austenite with temperature was found. The instantaneous and mean linear thermal expansion coefficients at 1350 K were estimated to be $2.12 \times 10^{-5}\ K^{-1}$ and $1.72 \times 10^{-5}\ K^{-1}$, respectively. The measured enthalpy data were made use of in estimating heat capacity, entropy and Gibbs energy values. The estimated isobaric heat capacity C_p at 298 K was found to be $406\ J\ kg^{-1}\ K^{-1}$. An integrated theoretical analysis of the thermal expansion and enthalpy data was performed to obtain approximate values of bulk modulus as a function of temperature.

PACS: 65.40.−b; 65.40.Ba; 81.05.Bx

1. Introduction

Austenitic stainless steels, as a class of engineering materials, possess an attractive combination of physical and mechanical properties, and as a result have wide-ranging applications as well. They are the preferred candidates for the core components of a liquid metal cooled nuclear fast reactor. Apart from the general requirements expected of any high temperature structural material, the highly radioactive environment of a fast reactor imposes specific demands on nuclear grade stainless steels. Among these, ensuring adequate swelling resistance at fast neutron flux, as well as maintaining the required strength and ductility levels, are of paramount importance in securing the overall structural integrity of the core components. Based on the current understanding of irradiation induced void swelling in Fe–Ni–Cr–C alloys [1], subtle modifications in composition, in addition to an adroit manipulation of the microstructural elements have been resorted to in designing nuclear grade stainless steels. The material of the present study, namely alloy D9 is one such candidate, wherein the base composition of a typical AISI 316 stainless steel is altered in favour of a slightly higher Ni to Cr ratio, and an enhancement in the silicon content by a small amount [2]. More importantly, the compositional

* Corresponding author. Tel.: +91 4114 280 306; fax: +91 4114 280 081.
E-mail address: sraju@igcar.ernet.in (S. Raju).

0022-3115/$ - see front matter © 2005 Elsevier B.V. All rights reserved.
doi:10.1016/j.jnucmat.2005.06.009

tailoring of alloy D9 is characterized by the fact that it contains explicitly added titanium in amounts that are a small multiple of the carbon content [2]. It is believed that during the actual in-pile conditions, the presence of titanium in the matrix is crucial for binding a portion of the dissolved carbon in the form of tiny TiC precipitates [3]. Further, a heterogeneous nucleation of these TiC particles is facilitated by introducing a dislocation substructure to the austenite matrix through a controlled amount of prior cold work [4]. It is held, that the TiC-matrix interfaces serve as sinks for the radiation induced point defects and thus contribute to enhancing the swelling resistance of alloy D9 [3,4].

For the Indian Prototype Fast Breeder Reactor (PFBR) programme, several variants of alloy D9 with the Ti/C ratio in the range 4–8 were studied in the recent past with respect to their mechanical and forming properties [5–8]. But the thermophysical properties of these alloys remain to be studied in detail. Since accurate thermal property data are needed from the point of view of enabling a confident design of engineering components, it was decided to study the thermal properties of an indigenously developed variety of alloy D9. Accordingly, we have investigated in the present study the temperature variation of lattice parameter and enthalpy by high temperature X-ray diffraction (HTXRD) and inverse drop calorimetry techniques, respectively. The results of these experiments are reported in this paper.

The organization of this paper is as follows. In Section 2, the essential details of the experimental methods are presented. In particular, the procedures adopted for the calibration the HTXRD spectra and the drop calorimetry data are discussed in detail. This is followed in Section 3 by the systematic presentation of experimental results. Section 4 deals with an integrated theoretical analysis of thermal expansion and enthalpy data obtained in the present study in light of a novel thermodynamic approach. This theoretical analysis is based on the existence of an isobaric linear scaling relation between enthalpy and specific volume [9,10]. In the final section, the findings of this study are listed.

2. Experimental details

The alloy D9 used in the present study was procured from MIDHANI India, in the form of rods of about 2.5 cm in diameter. The compositional details, as determined by standard wet chemical methods and by direct reading optical emission spectrometry, are listed in Table 1. For comparison, the nominal compositions of other related varieties of austenitic stainless steels are also listed. The bulk density of the sample, as measured by a standard immersion technique is found to be 8.1 g cm^{-3}. For both X-ray and drop calorimetry investigations, the as-procured material was solution annealed at 1323 K in argon atmosphere for approximately 1 h.

2.1. High temperature X-ray diffraction (HTXRD) studies

For HTXRD studies thin slices were cut from the annealed rod and then cold rolled to obtain foils of thickness ranging from 75 to 100 μm. These foils were subsequently strain relieved by annealing them at 1323 K for about 30 min in an argon atmosphere. The HTXRD studies were performed in a Philips-X'pert MPD® system, equipped with the Büehler® high vacuum heating stage. Typical instrument related parameters were: operating voltage of 40 kV; current of 45 mA for the X-ray tube; scan speed of 0.02° s^{-1} with a counting time of 6 s per step and an angular range (2θ) of 20–80°. The heating stage consisted of a thin (~80 μm) resistance heated tantalum foil, on top of which the sample was placed. The temperature was measured by a W–Re thermocouple, which was spot-welded to the bottom of the tantalum heater. The temperature was controlled to an accuracy of about ±1 K. The diffraction studies were performed using CuK_α radiation in the Bragg–Brentano geometry, at a temperature interval of 50 K up to 1350 K. A heating rate of 1 K min^{-1} and a holding time of 60 min at each temperature of measurement were adopted. The specimen stage was flushed with high purity argon before the start of every experimental run and a vacuum level of about 10^{-5} mbar was maintained throughout the experiment. Owing to the intrinsic design of the heating stage and also due to the residual non-planarity of our rolled foil sample, there prevailed an unavoidable temperature drop at the heater–sample interface. In addition, there was also present a temperature gradient across the section thickness of the sample. This temperature gradient could be minimized by using a thin foil, although too thin a foil resulted in buckling or sample geometry deformation at high temperatures. Acquisition and preliminary analysis of data were performed by the Philips X'pert Pro® software, although at a latter stage, we resorted to an independent processing of the raw data for a precise determination of the peak position. The 2θ calibration for the room temperature run was made with the help of silicon and α-alumina standards. However, for high temperatures, we co-recorded the XRD pattern of the tantalum heater together with sample reflections. This was made possible by cutting a very narrow keyhole-like wedge in the sample, exposing a good amount of sample as well as the underlying tantalum heater surface to the incident X-rays. The experimentally obtained reflections for tantalum, vis-a-vis the recommended temperature dependent lattice parameter data, taken from the assessment of Reeber and Wang [11] were used to calibrate the apparent shift introduced

Table 1
Nominal chemical composition[a] in weight percent of alloy D9 investigated in the present study, listed together with the compositional details of other related austenitic stainless steels

Element	304[b]	304L[c]	316[b]	316 LN[d]	321[e]	D9[f]	D9[g]
Ni	9.7	9.3	11.7	12.5	9.0–12.0	14.9 ± 0.5	15.5
Cr	18.4	18.5	16.8	18.0	17.0–19.0	14.7 ± 0.5	13.5
Mn	1.4	1.16	1.9	1.6–2.0	<2.00	1.3 ± 0.05	2.0
Mo		0.15	2.1	2.7		2.2 ± 0.05	2.0
Cu		0.1	0.2	1.0		<0.050	
Ti					$\geqslant 5 \times$%C	0.18 ± 0.006	0.25
Nb						<0.07	
V						0.045 ± 0.005	
Co		0.18		0.25		0.03 ± 0.005	
Al						<0.034	
Sn						<0.004	
W						0.005	
Si	0.6	0.7	0.4	0.05	$\leqslant$1.00	0.65 ± 0.05	0.75
C	0.02	0.022	0.05	0.03	$\leqslant$0.08	0.05 ± 0.005	0.04
N		0.010		0.08		<0.04	
P	0.02	0.010	0.03	0.035	$\leqslant$0.045	0.008 ± 0.001	
S	0.01	0.011	0.02	0.025		0.005 ± 0.003	
B				0.002			
As						<0.006	
Fe	Balance	Balance	Balance	Balance	Balance	Balance	
Density at ~300 K (kg m^{-3})	~7860	~8000	~7970	~7966		~8200[h]	

[a] It must also be stated that in general there is considerable scatter in the stated compositions of the same steel by different investigators and what is quoted here are those compositions for which experimental thermophysical property data are available.
[b] From Ref. [31].
[c] From Refs. [20,24].
[d] From IGCAR internal report (PFBR/01000/DN/1000).
[e] From Ref. [33].
[f] Determined in this study using direct reading optical emission spectrometry.
[g] From Ref. [21].
[h] Density determined in the present study using immersion technique.

to the recorded 2θ values, due to sample geometry deformation. This procedure, however, did not yield any absolute, or for that matter, separable estimates of the total error in the recorded 2θ, as distinctly arising from the temperature difference between the heater foil and the sample and that due to sample distortion upon possible buckling at high temperature. Four HTXRD runs on samples of slightly varying thickness, in the range 75–100 μm were performed. Of these, one of the runs involved concurrent recording of reflections from both the sample and tantalum heater, and the other three involved only the sample reflections. Thus, in addition to ensuring proper averaging of the 2θ values, we could also estimate the correction to the measured 2θ values to get the actual ones. As a final point, we would like to mention that repeated XRD runs performed on a specific sample resulted in quite reproducible results.

2.2. Drop calorimetry studies

For enthalpy measurements, the bulk sample was cut into smaller chips weighing about 50–100 mg. The mass of each sample was precisely determined to an accuracy of ±0.1 mg using a precision balance. The drop calorimetry measurements were performed with SETARAM-HTC 96® high temperature calorimeter. The furnace and the experimental chamber of this equipment were evacuated initially and were subsequently purged with pure argon before the commencement of an experimental run. An inert atmosphere was maintained throughout the experiment to prevent the evaporation of carbon from the graphite furnace at high temperatures. During the preparatory stages, highly pure dry alumina powder was filled up to two-thirds of a small recrystallized alumina crucible housed at the bottom of the experimental chamber. This alumina bed was heated by the surrounding graphite furnace. The alloy D9 samples were placed in individual specimen slots, located with the top assembly of the experimental chamber. In addition, standard samples of α-Al_2O_3, supplied by SETARAM were also loaded into the remaining slots of the specimen carousel. The temperatures of the furnace and that of the experimental chamber were independently measured by Pt–Pt/Rh thermocouples.

The whole experiment, other than the act of dropping of the sample was controlled through a computer that is connected to the main equipment through a proprietary interface module.

Previously weighed and cleaned samples were loaded in to the specimen holder that was kept at the ambient temperature, namely 295 K. The furnace was then gradually heated to the desired experimental temperature under argon gas cover at a rate of 10 K per minute. Once the temperature of the alumina bed has reached the preset value to within an accuracy of ±0.1 K, the samples were dropped from their respective slots through a guiding ceramic tube into the hot alumina bed. The heat absorbed by the specimen upon its drop from ambient temperature into the preheated alumina bed was accurately quantified by monitoring the change in temperature as well as the power supplied to the bed as a function of time. This data acquisition was conducted automatically by the proprietary software. The exercise was repeated by dropping α-Al_2O_3 standards under identical conditions. Presuming negligible heat loss due to radiation, and besides invoking quasi-adiabatic conditions to prevail in the experimental chamber, $Q_S(T)$, the heat energy transported from the bed to the sample may be written as follows [12]:

$$Q_S(T) = C(T)(m_S/M_S)(H_T - H_{295})_S. \quad (1)$$

In Eq. (1), m_S is the actual mass of the sample, M_S its molar mass, $H_T - H_{295}$ is the measured enthalpy increment with respect to 295 K, which is the reference temperature and C is a temperature-dependent calorimeter constant. The latter quantity may be obtained from the heat change measured with respect to the standard alumina reference (Q_R) and from the knowledge of its critically assessed enthalpy values [13]. Thus,

$$Q_R(T) = C(T)(m_R/M_R)(H_T - H_{295})_R. \quad (2)$$

In the above expression, m_R and M_R denote, respectively, the actual and the molar mass of alumina reference, which is taken to be 101.96 g mol^{-1} [13]. For alloy D9, the enthalpy values are measured at several temperature intervals in the range 400–1100 K. A minimum of two runs is performed at each temperature with samples of slightly different mass. These values showed a fair degree of agreement. To ensure a high degree of reliability, we also measured the enthalpy of OFHC grade copper (>99.99% pure) up to a temperature of 1100 K. A good agreement was obtained between the values measured in the present study and reported values [14,15], including the latest assessment by the authors [9]. At temperatures higher than about 1250 K, the alloy D9 samples showed mild signs of oxidation. In any case, the present measurements did not exceed this temperature limit.

3. Results

3.1. Lattice thermal expansion data

In Fig. 1, a stack of XRD profiles obtained with alloy D9 for different temperatures is presented. This was a typical HTXRD run made with ~100 μm thick foil. The lattice parameter a, was estimated from the three *fcc* reflections, namely (1 1 1), (2 0 0) and (2 2 0). Finally, an effective high angle corrected lattice parameter at each temperature was obtained by the standard Nelson–Riley extrapolation procedure [16]. In Fig. 2, the lattice parameter data as a function of temperature are plotted for three individual runs taken with foils of slightly varying thickness. Although a certain amount of scatter is noticed among the data obtained in the three runs, an overall smooth variation of the lattice parameter with temperature is clearly evident. As mentioned earlier, one possible reason for the scatter in the data could be the varying amount of sample buckling, in addition to the temperature difference prevailing at the sample-heater interface. The extent of this sample geometry distortion induced shift in 2θ is a very difficult issue to be quantified in rigorous terms. However, we fitted all the data from the three typical experimental runs to a

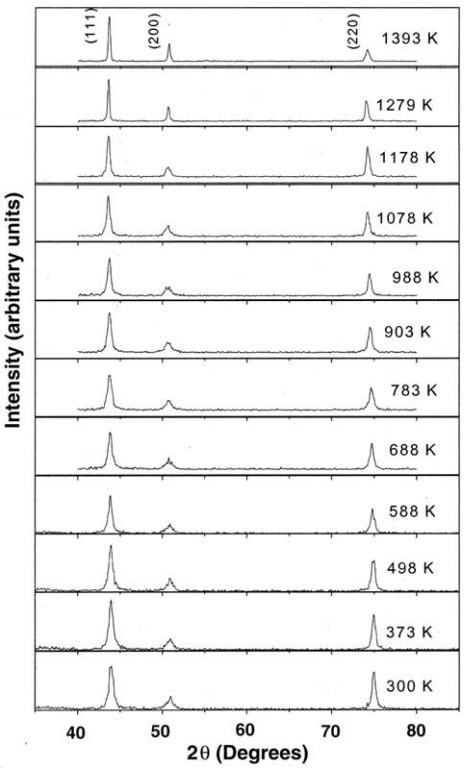

Fig. 1. High temperature X-ray diffraction profiles of alloy D9 taken at different temperatures.

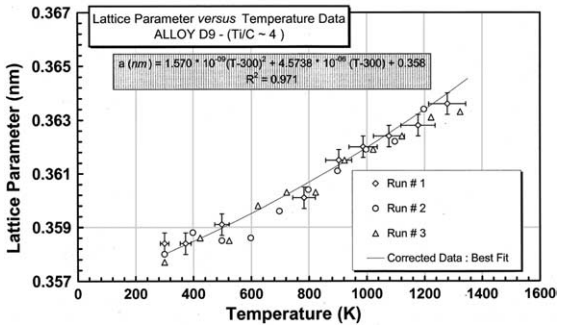

Fig. 2. The variation of the corrected lattice parameter of alloy D9 with temperature, are presented for three different experimental runs.

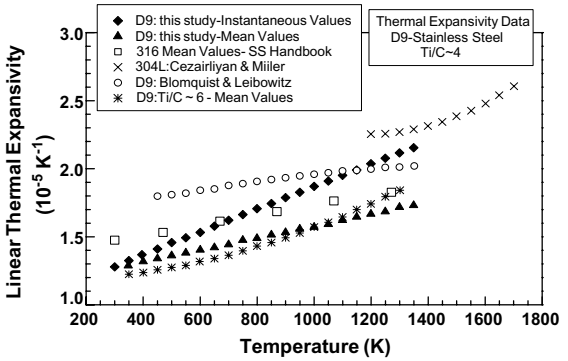

Fig. 3. The instantaneous and mean linear thermal expansion coefficients of alloy D9, estimated from the present lattice parameter data are plotted together with the reported values for 316, 304L and the American version of D9 [19–21].

second-degree polynomial in temperature increment $(T-300)$. The resulting fitted data were further corrected for possible errors in the measured temperature using the co-recorded tantalum reflections. These corrected data are marked as the best-fit line in Fig. 2. This calibration method relied on the assumption that the apparent errors in the measured 2θ behaved identically for both tantalum and the sample. Although lacking in sophistication, this procedure yielded a fair amount of success in our recent thermal expansion studies on stainless steel and inconel 600 [17,18]. It was estimated that an uncertainty of ± 25 K in temperature resulted in a change of lattice parameter of about ± 0.00275 nm for $T \geqslant 800$ K. For lower temperatures, the error was much less. The relative error in 2θ was calibrated by using silicon and α-alumina standards.

For the purpose of estimating thermal expansion, the corrected lattice parameter data were fitted to a second-degree polynomial in the temperature increment $(T-300)$

$$a\ (\mathrm{nm}) = 0.358 + 4.574 \times 10^{-6}(T-300) + 1.570 \times 10^{-9}(T-300)^2. \quad (3)$$

Once the lattice parameter was known as a function of temperature, it became possible then to estimate the instantaneous (α_L-instantaneous), mean (α_L-mean) and relative linear thermal expansion coefficients (α_L-relative) by the following relations:

$$\alpha_L\text{-instantaneous} = (1/a_T) \times (\mathrm{d}a_T/\mathrm{d}T), \quad (4)$$

$$\alpha_L\text{-relative} = (1/a_{300}) \times (\mathrm{d}a_T/\mathrm{d}T), \quad (5)$$

$$\alpha_L\text{-mean} = (1/a_{300}) \times \{(a_T - a_{300})/(T-300)\}. \quad (6)$$

In Fig. 3, the mean and the instantaneous linear thermal expansivity values obtained in the present study were plotted as a function of temperature. These values were also listed in Table 2. For the sake of comparison, we also report in Fig. 3, the data gleaned from the literature on 316, 304L [19,20] and on a slightly different composition of D9 studied by Leibowitz and Blomquist [21]. It might be remarked that notwithstanding the diverse sources of errors that are invariably associated with HTXRD experiments, the thermal expansion values obtained in the present study for alloy D9 showed an overall agreement with the data on related 316, 304L and D9 stainless steels. While the present estimates based on HTXRD characterized the lattice thermal expansion of alloy D9, the data on other steels, taken from literature were characteristic of bulk thermal expansion, obtained by dilatometry. This fact partly accounts for the relatively lower values of thermal expansivity obtained in the present study for the present alloy D9, as compared to the corresponding estimate for its American counterpart [21]. Moreover, it must also be stressed that the compositions of these two similar nuclear grade stainless steels are by no means identical (see Table 1). It must also be noted that the present thermal expansivity estimates compare well with our earlier experimental data on another variant of alloy D9 with Ti/C = 6 [17]. However, for $T \geqslant 1000$ K, the D9 with slightly higher titanium content showed a steep rise in its thermal expansion behavior. At this stage, the role of higher titanium in the matrix on thermal properties is not clear; but it appears that a slightly larger titanium content can have quite surprisingly distinct effects on high temperature thermophysical properties. Further experiments on alloy D9 with different Ti/C ratio are required to establish a definite systematics.

3.2. Enthalpy data

In Fig. 4, the measured enthalpy increment $(H_T - H_{295})$ values for alloy D9 were plotted together with the currently available estimates on AISI 316 and 347 stainless steels [22–24]. It is clear that the enthalpy values obtained in the present study for alloy D9 are

Table 2
The lattice parameter (a), instantaneous (α_L-inst), relative (α_L-rel) and mean (α_L-mean) linear thermal expansion coefficients of alloy D9 obtained in this study are tabulated as a function of temperature

T (K)	a (nm)	Specific volume (10^{-4} m^3 kg^{-1})	α_L instantaneous (10^{-5} K^{-1})	α_L relative (10^{-5} K^{-1})	α_L mean from 300 K (10^{-5} K^{-1})	Mean thermal expansion from 300 K (%)
300	0.3595	1.224	1.28	1.28		
350	0.3598	1.226	1.32	1.32	1.30	0.06
400	0.3601	1.229	1.36	1.37	1.32	0.13
450	0.3604	1.231	1.41	1.41	1.34	0.20
500	0.3607	1.234	1.45	1.45	1.37	0.27
550	0.3610	1.237	1.49	1.50	1.39	0.35
600	0.3613	1.240	1.53	1.54	1.41	0.42
650	0.3616	1.242	1.58	1.58	1.43	0.50
700	0.3620	1.245	1.62	1.63	1.45	0.58
750	0.3623	1.248	1.66	1.67	1.47	0.66
800	0.3627	1.242	1.70	1.72	1.50	0.75
850	0.3630	1.282	1.75	1.76	1.52	0.84
900	0.3634	1.255	1.79	1.80	1.54	0.92
950	0.3638	1.258	1.83	1.85	1.56	1.02
1000	0.3641	1.262	1.87	1.89	1.58	1.11
1050	0.3645	1.265	1.91	1.94	1.61	1.20
1100	0.3649	1.269	1.95	1.98	1.63	1.30
1150	0.3653	1.272	1.99	2.02	1.65	1.40
1200	0.3657	1.280	2.04	2.07	1.67	1.50
1250	0.3662	1.284	2.08	2.11	1.90	1.61
1300	0.3666	1.288	2.12	2.15	1.20	1.72

The specific volume is estimated by assuming a value of 56.41 for the average molecular weight of alloy D9. This value is similar to that of 316 stainless steel.

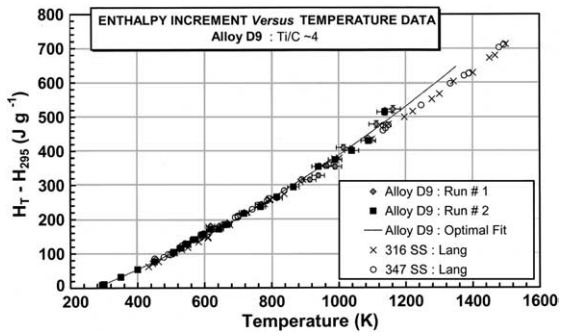

Fig. 4. The measured enthalpy values for alloy D9 are plotted together with the corresponding data on 316 and 347 stainless steels, taken from literature [22].

in excellent agreement with the data on related grades. However for temperatures exceeding about 850 K, alloy D9 exhibited systematically higher values than both 316 and 347. Before proceeding further, it must be mentioned that to the best of our knowledge, we are not aware of any information on experimentally determined enthalpy data for alloy D9. The enthalpy data obtained in the present study in the temperature range 370–1300 K were fitted to the following expression:

$$H_T - H_{295}\ (\mathrm{J\,g^{-1}}) = -93.76 + 0.2919T + 1.896 \times 10^{-4}T^2 + 1.345 \times 10^{-7}/T. \quad (7)$$

Eq. (7) fits the experimental data with a R^2 value of 0.995 in the temperature range 370–1300 K. The isobaric heat capacity C_p was readily obtained by differentiating the above expression with respect to temperature

$$C_p\ (\mathrm{J\,g^{-1}\,K^{-1}}) = 0.2919 + 3.792 \times 10^{-4}T - 1.345 \times 10^{-7}/T^2. \quad (8)$$

The C_p value at 300 K, as estimated from the above expression turns out to be 406 J kg^{-1} K^{-1}. This was found to be slightly lower than the value of 412 J kg^{-1} K^{-1}, reported for 316 stainless steel [22,23]. Once C_p had been known as a function of temperature, it was then possible to calculate entropy (S_T) as well as Gibbs energy (G_T) from their respective thermodynamic definitions

$$S_T = S_0 + \int (C_p/T)\,\mathrm{d}T \quad (9)$$

and

$$\Delta G_T = \Delta H - T\Delta S. \quad (10)$$

Owing to the lack of low temperature heat capacity data on alloy D9, we could not obtain an experimentally based estimate for S_0, the standard entropy at 298 K

Table 3
The thermodynamic functions of alloy D9 estimated in the present study from the measured enthalpy values are tabulated

T (K)	$H_T - H_{300}$ (fit values) (J g^{-1})	C_p (J Kg^{-1} K^{-1})	$S_T - S_{300}$ (J Kg^{-1} K^{-1})	$G_T - G_{300}$ (J Kg^{-1})
350	31.64	424.62	63.96	−1772.37
400	53.35	443.58	121.89	−6584.90
450	76.00	462.54	175.24	−14174.58
500	99.61	481.50	224.95	−24337.28
550	124.16	500.46	271.73	−36909.92
600	149.66	519.42	316.09	−51759.22
650	176.10	538.38	358.41	−68774.17
700	203.50	557.34	399.01	−87860.93
750	231.84	576.30	438.11	−108939.08
800	261.13	595.26	475.90	−131938.95
850	291.37	614.22	512.56	−156799.60
900	322.56	633.18	548.20	−183467.27
950	354.69	652.14	582.95	−211894.20
1000	387.77	671.10	616.88	−242037.64
1050	421.81	690.06	650.08	−273859.14
1100	456.78	709.02	682.62	−307323.89
1150	492.71	727.98	714.56	−342400.29
1200	529.59	746.94	745.94	−379059.45
1250	567.41	765.90	776.82	−417274.91
1300	606.18	784.86	807.22	−457022.33

from literature. Under this circumstance, we invoke a general assumption that the thermal properties of closely related stainless steels do not show much of a variation to the first order of approximation. Under such conditions, it may be said that in the absence of reliable experimental data for a new candidate, the value corresponding to a well-studied homologous member of the family may be taken as a representative of the entire class itself. It is in this spirit, we have chosen the value for the S_0 of alloy D9 as 2.93 J kg^{-1} K^{-1}. This value corresponds to the standard entropy of 316 stainless steel at 298 K [25]. It must be recalled that the composition of alloy D9 is essentially derived from 316 stainless steel. In Table 3, the thermodynamic functions of alloy D9 estimated in the present study are tabulated.

4. Discussion

4.1. General remarks

Two issues merit a detailed clarification in discussion of present results. In the first, it must be mentioned that what is measured in the present study is the relative lattice thermal expansion of the austenite as a function of temperature, where as the microstructure of alloy D9 is one of consisting finely dispersed TiC particles in the *fcc* matrix. Going by our XRD results, it is clear that the volume fraction of these TiC precipitates is not appreciable enough to record their presence in the X-ray diffraction profile. Nevertheless, their presence as nanoscale particles was conformed through high-resolution electron microscopy studies [34]. The presence of TiC has two fold effects on the lattice parameter of austenite matrix. Being a mechanically hard phase (TiC has a higher shear modulus than austenite) and by virtue of the fact that these particles are fairly uniformly dispersed in the matrix, it is quite likely that the austenite matrix is in a state of compression. We may call this as chemical compression, as opposed to uniform hydrostatic compression that is characteristic of a typical high-pressure experiment. We believe that this chemical compression effect will not get relieved to any appreciable extent even at high temperatures, especially since TiC particles are fairly stable at these temperatures. In view of this, what was monitored in the present study had been the lattice expansion of this strained austenite phase. It is true that TiC although present in only small volumes, also experiences a net thermal expansion. But, we may discount this phenomenon, as its thermal expansivity is one order less than that of austenite. In any case, even the small expansion of hard TiC would only serve to aggravate the interfacial strain of the austenite/TiC aggregate. In the present experiment, since the presence of TiC was not noticed in the HTXRD spectrum, we have effectively ignored the role of these precipitates in affecting the thermal expansion behavior of alloy D9. In other words, it is only the constrained thermal expansion behavior of alloy D9 that is discussed in this study. This point must be kept in mind, while enacting a comparison with other results.

The second point that must be brought to discussion table is the fact that there is in general a paucity of information on the thermophysical properties of alloy D9. Using dilatometry, Blomquist and Leibowitz studied the bulk thermal expansion behavior of a D9 stainless steel that has a slightly different composition from the presently studied one [21]. In addition, we have previously elucidated the thermal expansion behavior of another D9 variety that had a Ti/C ratio of about six [17]. The results of these studies, as shown in Fig. 3, bring out the fact that the thermal expansion behavior of alloy D9 are invariably subject to certain scatter. As mentioned before, the mild upward turn seen in the thermal expansivity of alloy D9 with Ti/C = 6 (see Fig. 3) could not be obtained in the present study performed with a steel having Ti/C = 4. On the other hand the thermal expansion values obtained in the present study compare fairly well with that of 316 stainless steel [19]. However, the bulk thermal expansion characteristics of 304L stainless steel, as studied by Cezairliyan and Miiller [24] reveal a marked rise at high temperatures, approaching the melting point. This could not be confirmed in the present study, as the maximum temperature reached in the present experiment did not exceed 1350 K. It was also found that any prolonged hold at temperatures exceeding about 1250 K in the high temperature X-ray diffraction stage resulted in appreciable oxidation of the alloy and this added to the intrinsic difficulty in obtaining a good clean XRD pattern at high temperatures. It is likely that this pronounced rise seen in high temperature thermal expansivity of austenitic stainless steels could arise from the proliferation of defects as well as due to the domineering influence of lattice anharmonicity.

The above picture seems to derive support from the behavior of the enthalpy values measured in the present study (see Fig. 4). It is clear that with respect to the base 316 stainless steel data, the enthalpy of alloy D9 exhibits a steady rise for temperatures exceeding about 850 K. As discussed in the previous section, it is not clear as to how much of this increase is an intrinsic property of the austenite matrix or it stems from the presence of a small fraction TiC particles in an otherwise clear austenite matrix. In addition, it is also possible that an onset of lattice anharmonicity or the proliferation of point defects at high temperatures may induce further complications at high temperatures. Clearly further studies are required for a better elucidation of this point.

4.2. Combined analysis of enthalpy and volume data

It is a well-known fact that for temperatures exceeding the Debye characteristic temperature (θ_D), the thermal Grüneisen parameter (γ_G) for most of the condensed systems is fairly temperature-insensitive. This suggests that there is an interesting trade-off between the temperature dependencies of thermal and elastic quantities involved in the thermodynamic definition of γ_G [26]

$$\gamma_G = (\alpha_V V/C_p) \times B_S. \tag{11}$$

It is obvious that a rise in temperature brings about an increase in α_V, V, and C_p, and a decrease in B_S, the adiabatic bulk modulus. During the course of his pioneering studies on the thermal physics of condensed matter, Grüneisen argued that in addition to γ_G, the ratio (λ) between volume thermal expansivity (α_V) and isobaric specific heat (C_p) was also a temperature-independent quantity [27,28]. The full thermodynamic implications of these hypotheses have recently been explored by us to bring out explicitly the multifarious interrelationships that are possible between thermal and elastic quantities [9,10,27,28]. One of the useful outcomes of these studies is the finding that, in the place of the classical Grüneisen approximation concerning λ, it is profitable to invoke a linear scaling relation between enthalpy and thermodynamic volume [9]. Incidentally, the original hypothesis of Grüneisen concerning constant λ, implies that the enthalpy varies linearly as the logarithm of thermodynamic volume [27]. That is to say,

$$\lambda = (\alpha_V/C_p) = (\partial \ln V/\partial H)_p, \tag{12}$$

is a temperature-independent constant. This fact, taken *together* with the temperature insensitivity of γ_G, implies that the energy product $B_S V$ must also be temperature-independent (vide Eq. (11)). It has now been established that both γ_G as well as λ are indeed temperature-sensitive in a mutually coupled fashion [9,28]. Further, it has recently been demonstrated that a number of systems exhibit a linear scaling relationship between enthalpy and volume under constant pressure conditions. The interesting aspect about this scaling relation is that it allows for the temperature variation of both γ_G as well as λ to be expressed in simple terms [9,10]. In the present study, we apply this thermodynamic formalism for an integrated treatment of enthalpy and specific volume data obtained in the present study.

In Fig. 5, we have portrayed the response of the enthalpy change with respect to the corresponding change in specific volume. The effect of temperature on these two prominent themodynamic quantities is implicitly contained in this graph. In other words, each data point corresponds to a specific temperature and hence the linear correlation seen in Fig. 5 is an isobar. In the first, it is instructive to note the remarkable linear correlation between these two quantities. This correlation is significant in the present context, especially since it provides a means for estimating the adiabatic bulk modulus from purely thermal property data. The relevant physics is extensively dealt with in our recent paper and hence only a brief working account is recalled here [9].

Let us invoke the definition of thermal Grüneisen parameter (γ_G) as given in Eq. (11) and substitute

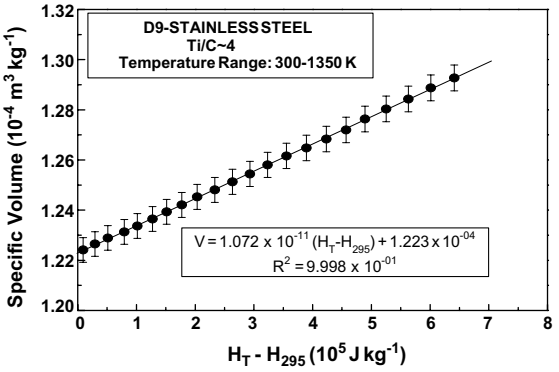

Fig. 5. The linear relationship between enthalpy and specific volume is illustrated with the data obtained in the present study.

therein the definitions of $\alpha_V = (\partial \ln V/\partial T)_p$, and $C_p = (\partial \Delta H/\partial T)_p$ to obtain the following relation:

$$\gamma_G/B_S = (\partial V/\partial \Delta H)_p. \tag{13}$$

It emerges from the above expression that a linear correlation between enthalpy increment (ΔH) and specific volume (V) signifies the temperature insensitivity of the ratio γ_G/B_S. In other words we may write the following approximation:

$$\gamma_G/B_S = \gamma_0/B_0, \tag{14}$$

where γ_0 stands for the Grüneisen parameter at the reference temperature (T_0) and B_0 is the corresponding value of the adiabatic bulk modulus. A similar identity regarding the temperature independence of γ_G/B_T is readily obtained, if C_p is replaced by C_V in defining γ_G. In either case, the physical significance of this deduction is that the effect of temperature on both enthalpy and molar volume being commensurate, the variation of γ_G with temperature, albeit expected to be small, is entirely decided by the temperature sensitivity of bulk modulus. Since it is known that $B_S(T)$ is one of usually decreasing with temperature, it follows that γ_G is also decreasing with temperature. It must be mentioned that this statement is basically a high temperature approximation and is obeyed as such for temperatures greater than the Debye temperature (θ_D). In addition, the system under consideration should not derive appreciable contribution from extraneous factors like point defects and other electronic degrees of freedom that only contribute to destroy the linearity of the relationship between enthalpy and volume.

Now coming to the present context, a practical appeal of Eq. (13) would be in estimating the temperature dependent bulk modulus from a combined knowledge of the slope of the V–ΔH curve (Fig. 5) and γ_G. Of these, the former quantity namely, $(\partial V/\partial \Delta H)_p$ is found to be 1.072×10^{-11} m^3 J^{-1}. The temperature variation of γ_G is the most difficult one to quantify accurately. In the present study, the temperature variation of γ_G is treated in terms of its isobaric volume dependence. Thus, differentiating the Grüneisen relation, as given in Eq. (11) with respect to temperature at constant pressure yields the following thermodynamic relation [28]:

$$(\partial \ln \gamma_G/\partial \ln V)_p - (\partial \ln \lambda/\partial \ln V)_p + \delta_S = 1. \tag{15}$$

In the above expression, which is an exact thermodynamic identity, $\delta_S = -(\alpha_V B_S)^{-1} \times (\partial B_S/\partial T)_p$, is the adiabatic Anderson–Grüneisen parameter and $\lambda = \alpha_V/C_p$ is the Grüneisen ratio [29]. Further, the fact that V and ΔH are linearly related implies that $(\partial \ln \lambda/\partial \ln V)_p = -1$ [30]. Therefore, within scope of the present theoretical framework, we obtain,

$$(\partial \ln \gamma_G/\partial \ln V)_p \approx -\delta_S. \tag{16}$$

Alternately in the integrated form, we may write the following power law expression for γ_G:

$$\gamma_G = \gamma_0 (V/V_0)^{-\delta_S}. \tag{17}$$

Combining Eqs. (14) and (17), the following relation characterizing the isobaric volume dependence of B_S is readily obtained:

$$B_S = B_0 (V/V_0)^{-\delta_S}. \tag{18}$$

Therefore the estimation of temperature dependent B_S from thermal expansion data entails only the specification of two quantities, namely B_0 and δ_S. For alloy D9, there are no experimental data available on either of these two quantities. Therefore, following the law of homologous behavior among solids of similar physical chemistry, we assume the B_0 and δ_S values of 316 stainless steel to be valid for alloy D9 as well. These values are taken as: $B_0 = 154$ GPa [31] and $\delta_S = 5.5$ [32]. The value of γ_0 may be estimated from Eq. (13) using the slope of the curve of Fig. 5 and B_0. This turns out to be 1.65. This is fairly close to the value of 1.74 deduced for 316 stainless steel based on shock wave data [32]. The temperature dependent values of adiabatic bulk modulus and Grüneisen parameter estimated via Eqs. (18) and (17), respectively, are tabulated in Table 4. At this juncture, it must be borne in mind that the bulk modulus obtained in the present study are only plausible estimates, especially since they are based on the validity of the linear scaling relation between enthalpy and thermodynamic volume. Such a linear scaling, although clearly exhibited by the experimental data obtained in the present study, is nevertheless subject to the uncertainties inherent of the high-temperature thermal property data. In other words, there is an intrinsic error margin associated with the slope of the curve in Fig. 5. In view of this point, extrapolating the validity of the linear scaling up to melting point (T_m) may be fraught with some uncertainty. Besides, it is known that at

Table 4
The temperature dependent adiabatic bulk modulus (B_s) values and the thermal Grüneisen parameter (γ_G) calculated in the present study using the linear scaling relationship between enthalpy and specific volume (Fig. 5) are tabulated

T (K)	γ_G	B_s (GPa)
300	1.65	154
350	1.63	152
400	1.61	151
450	1.60	149
500	1.58	147
550	1.57	145
600	1.54	144
650	1.52	142
700	1.50	140
750	1.48	138
800	1.46	136
850	1.44	134
900	1.42	132
950	1.40	130
1000	1.38	128
1050	1.35	126
1100	1.33	124
1150	1.31	122
1200	1.29	120
1250	1.27	118
1300	1.25	116

temperatures very close to the melting point, the proliferation of vacancies as well as the domineering influence of lattice anharmonicity contribute to a sharp fall in the elastic properties. Therefore it is likely that the perfect linearity witnessed in the moderately high temperature domain between the quantities (ΔH) and V may be rendered invalid at very high temperatures. Despite this limitation, we would like to emphasize that the high temperature bulk modulus values estimated in the present study, when viewed together with the experimental enthalpy and specific volume data constitute a fully thermodynamically consistent composite data set. In Fig. 6, the B_S values of alloy D9 estimated in the present study are plotted together with the corresponding values for 316 stainless steel. The latter values are calculated from the experimentally measured Young's modulus data and a temperature independent value of 0.285 for the Poisson ratio [19]. The fact that the B_S of alloy D9 bears close similarity to the B_T of 316 is noteworthy.

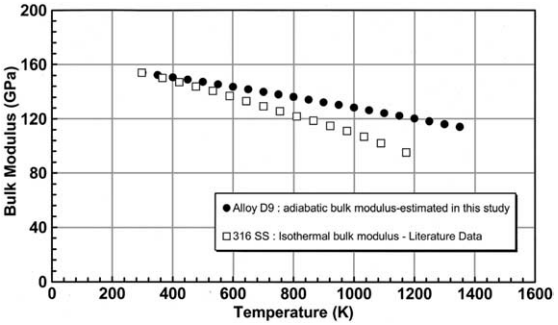

Fig. 6. The temperature variation of adiabatic bulk modulus of alloy D9 calculated in the present study is compared with the literature data on 316 stainless steel [19].

5. Conclusions

In the present study, lattice parameter and enthalpy values for a titanium modified nuclear grade austenitic stainless steel, namely alloy D9 have been measured in the temperatures range 300–1350 K. Both thermal expansivity and specific heat of alloy D9 obtained in the present study exhibited a good overall agreement with the reported values for other related austenitic stainless steels. A combined analysis of thermal expansion and thermochemical data has been made in the spirit of a modified Grüneisen formalism to obtain thermodynamically consistent estimates for high temperature bulk modulus.

Acknowledgments

The comments of the reviewer are helpful in enhancing the appeal of the paper. The authors sincerely acknowledge Dr Baldev Raj, Dr S.L. Mannan, Dr V.S. Raghunathan, Dr P.R. Vasudeva Rao and Dr M. Vijayalakshmi for the encouragement, and sustained support. Samples used in this study are courtesy of Dr P.V. Sivaprasad.

References

[1] F.A. Garner, Irradiation performance of clad and structural steels in liquid metal reactors, in: R.W. Cahn, P. Haasen, E.I. Kramer (Eds.), Materials Science and Technology: A Comprehensive Treatment, vol. 10 A, part-I, VCH, Weinheim, 1994, p. 420.
[2] S.L. Mannan, P.V. Sivaprasad, in: K.H.1. Buschow, R.W. Cahn, M.C. Flemings, B. Ilschner, E.J. Kramer, S. Mahajan (Eds.), Encyclopaedia of Materials Science and Engineering, vol. 3, Elsevier, New York, 2001, p. 2857.
[3] W. Kesternich, D. Meertens, Acta Metall. 34 (1986) 1071.
[4] S. Venkadesan, A.K. Bhaduri, P. Rodriguez, K.A. Padmanaban, J. Nucl. Mater. 186 (1992) 177.
[5] R. Sandhya, K.B.S. Rao, S.L. Mannan, R. Devanathan, Scripta Mater. 41 (1999) 921.
[6] V. Shankar, T.P.S. Gill, S.L. Mannan, A.L.E. Terrance, S. Sundaresan, Met. Mater. Trans. 31A (2000) 3109.
[7] R. Sandhya, K.B.S. Rao, S.L. Mannan, R. Devanathan, Int. J. Fatigue 23 (2001) 789.
[8] P.V. Sivaprasad, S.L. Mannan, Y.V.R K. Prasad, R.C. Chaturvedi, Mater. Sci. Technol. 17 (2001) 545.

[9] S. Raju, K. Sivasubramanian, E. Mohandas, Solid State Commun. 124 (2002) 151.
[10] S. Raju, K. Sivasubramanian, E. Mohandas, J. Alloys Compd. 375 (2004) 72.
[11] R.R Reeber, K. Wang, Mater. Sci. Eng. R 23 (1998) 101.
[12] J. Leitner, A. Strejc, D. Sedimidubsky, K. Ruzicka, Thermochim. Acta 401 (2003) 169.
[13] D.G. Archer, J. Phys. Chem. Ref. Data 22 (1993) 1441.
[14] V.Ya. Chekhovskoi, Y.V. Gusev, V.D. Tarasov, High Temp.–High Press. 34 (2002) 291.
[15] G.K. White, S.J. Col1ocott, J. Phys. Chem. Ref. Data 13 (1984) 1251.
[16] B.D. Cul1ity, Elements of X-ray Diffraction, 2nd Ed.., Addison Wesley, Reading, MA, 1978.
[17] R. Jose, S. Raju, R. Divakar, E. Mohandas, G. Panneerselvam, M.P. Antony, K. Sivasubramanian, J. Nucl. Mater. 317 (2003) 54.
[18] S. Raju, K. Sivasubramanian, R. Divakar, G. Panneerselvam, A. Banerjee, E. Mohandas, M.P. Antony, J. Nucl. Mater. 325 (2004) 18.
[19] R.M. Louthan, APT Materials Handbook, Savannah River Technology Center, Westinghouse, Savanna River, unpublished, as cited by M. Grujicic, H. Zhao, Mater. Sci. Eng. A 252 (1998) 117.
[20] A.P. Miiller, A. Cezairliyan, High Temp.–High Press. 23 (1991) 205.
[21] L. Leibowitz, R.A. Blomquist, Int. J. Thermophys. 9 (1988) 873.
[22] J.L. Lang, Thermodynamic and Transport Properties of Gases, Liquids and Solids, Graw-Hill, New York, 1959, p. 405.
[23] R.H. Bogaard, P.D. Desai, H.H. Li, C.Y. Ho, Thermochim. Acta. 218 (1993) 373.
[24] A. Cezairliyan, A.P. Miiller, Int. J. Thermophys. 1 (1980) 83.
[25] C.S. Kim, ANL-75-55 report, Argonne, IL, 1975, p. 1.
[26] G. Grimvall, Thermophysical Properties of Materials, North Holland, Amsterdam, 1991.
[27] S. Raju, E. Mohandas, K. Sivasubramanian, Scripta Mater. 44 (2001) 269.
[28] S. Raju, K. Sivasubramanian, E. Mohandas, Mater. Lett. 57 (2003) 3793.
[29] O.L. Anderson, Equations of State of Solids for Geophysics and Ceramic Sciences, Oxford University, Oxford, 1995.
[30] S. Raju, unpublished research, 2004.
[31] H. Ledbetter, J. Appl. Phys. 52 (1981) 1587.
[32] D. Gerlich, S. Hart, J. Appl. Phys. 55 (1984) 880.
[33] N.L. Perovic, K.D. Maglic, A.M. Stanimirovic, G.S. Vukovic, High Temp.–High Press. 27&28 (1995–1996) 53.
[34] A. Banerjee, R. Divakar, S. Raju, E. Mohandas, Unpublished Research, 2005.